POLARIZATION MEASUREMENTS OF JUPITER RADIO BURSTS AT 10·1 Mc/s

By R. L. Dowden*

[*Manuscript received May* 1, 1963]

Summary

At 10·1 Mc/s Jupiter bursts of both senses of circular polarization are readily observed. The algebraic mean axial ratio is a strong function of Jovian longitude. This is almost entirely due to variation with longitude of the relative proportion of bursts of opposite sense of polarization. If bursts of the two senses (L.H. and R.H.) are analysed separately the two mean axial ratios show little or no variation with longitude and are equal and opposite in sign. The axial ratio distribution and other observations are compared with the predictions of the Doppler-shifted cyclotron theory.

I. Introduction

Decametre radio bursts from Jupiter are elliptically polarized, usually in the right-handed (R.H.) sense. Observations by Bollhagen (Carr, personal communication) show that at 22 Mc/s, 99·4% of bursts are R.H. and 0·6% L.H., while at 16 Mc/s, 67% are R.H. and 33% L.H. No systematic variation of these ratios with longitude has been reported though "there are slight but apparently significant differences in the average polarizations" of bursts from the three main longitudes of emission (Carr *et al.* 1961). In contrast the measurements at 10·1 Mc/s described here show that, while the average for all longitudes is about 63% R.H. and 37% L.H., this ratio is strongly dependent on longitude,† varying from 95% R.H. at 270° to 17% R.H. at 85°.

II. Instrumentation

Jupiter bursts were received on a horizontal array of twenty pairs of crossed half-wave dipoles arranged in a 10×2 configuration with the long axis in the north-south direction. The half-power cone of the antenna beam cuts the celestial sphere in a banana-shaped curve which enclosed Jupiter for some two or three hours either side of transit throughout the period of observation. For symmetry (and minimum number of support poles) the two sets of dipoles were positioned in the NE.–SW. and NW.–SE. directions respectively, that is, both at 45° to the long axis of the antenna.

The transmission lines from the two orthogonal linear polarizations were interconnected by a quarter-wave line and matched to identical preamplifiers. The outputs of these, which were the amplified L.H. and R.H. components respectively, were sampled

* Ionospheric Prediction Service and the University of Tasmania; present address: Physics Department, University of Tasmania, Hobart.

† The longitude system used in this paper is the original System III of period 9h 55m 28·8s (Carr *et al.* 1958). To convert to the I.A.U. revised System III of period 9h 55m 29·37s (Carr *et al.* 1961), subtract 30° from the longitudes quoted in the text and the longitude scales of Figures 5, 6, and 7.

by a commercial communications receiver through a diode switch as shown in Figure 1. C.W. (e.g. communication and broadcast transmissions) interference was completely suppressed by using a "rectangular" i.f. band-pass filter of 4 kc/s bandwidth and by rapidly sweeping the second local oscillator through a range of about 12 kc/s. This

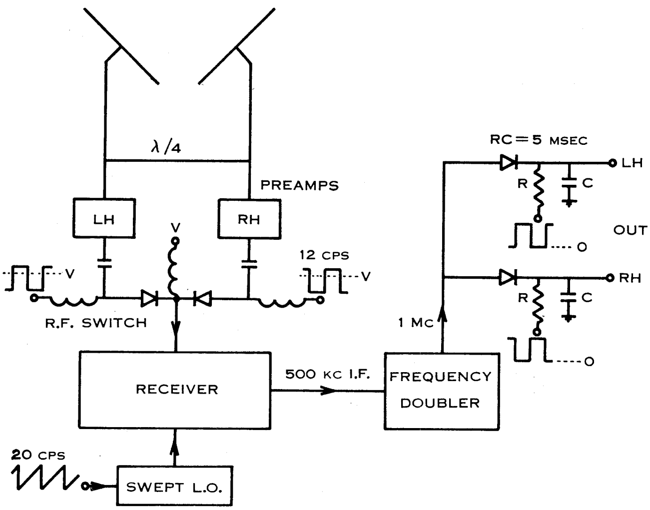

Fig. 1.—Block diagram of polarimeter.

converted c.w. interference to impulsive interference which could be suppressed, as explained later. Power linear detected outputs were obtained by doubling the intermediate frequency and using linear detectors. Voltage or field-strength linear outputs were also obtained by linear detection of the intermediate frequency before doubling

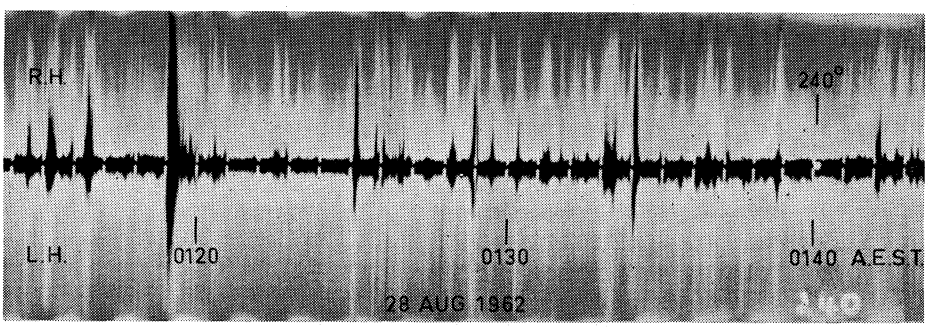

Fig. 2.—Typical C.R.O. record of 10·1 Mc/s Jupiter bursts.

(not shown). At each output the unwanted component of circular polarization was suppressed by applying a positive pulse to the "earthy" end of the detector load during the time the receiver sampled the unwanted component, as shown in Figure 1.

The wanted circular polarization component of Jupiter and Galactic radiation is separated from unwanted c.w. interference, wide-band impulsive interference (such as atmospherics), and the unwanted polarization component by using a system which records only the least signal occurring in a period of a few tens of milliseconds. The record shown in Figure 2 was obtained by connecting the L.H. and R.H. outputs to the deflection plates of a twin-beam cathode-ray oscilloscope. It is seen that all unwanted signals have been converted to unresolved pulses (filled-in white areas). Jupiter bursts appear as resolved (black) pulses and the Galactic component appears as a small steady level just above the zero level indicated by the one-minute time and zero marks. Pen recorders were also used by employing minimum reading circuits. This

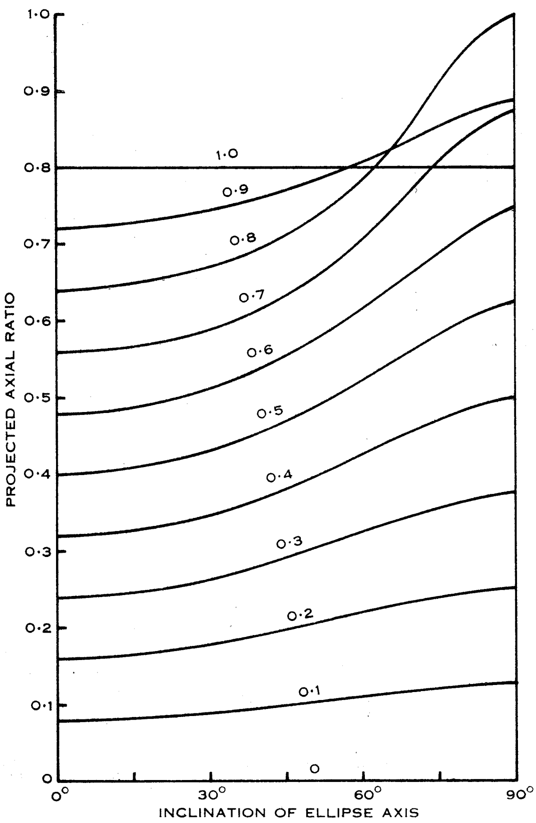

Fig. 3.—Apparent or projected axial ratio as a function of the inclination of the ellipse minor axis for various actual ratios and for an angle of incidence of 37°.

system is discussed in more detail elsewhere (Dowden 1963). A total of eight pen-recorder channels and six C.R.O. channels recording L.H., R.H., and L.H. minus R.H. components, using both power linear and voltage linear recording and different paper and film speeds were operated simultaneously. However, the two power linear C.R.O. channels recorded on 35-mm film moving at 6 in. per hour produced the best records, and only these are discussed here.

III. Axial Ratio Measurement

If Jupiter bursts are completely elliptically polarized and if the peak powers of the two components of a single burst are obtained, the apparent axial ratio is given by $\gamma = (r^{\frac{1}{2}}-1)/(r^{\frac{1}{2}}+1)$, where r = Peak power of L.H. component/Peak power of R.H. component.

However, with a horizontal antenna system as described above, the axial ratio measured is that of the horizontal components of the electromagnetic field, and thus that of the polarization ellipse projected onto the horizontal plane. The apparent or projected axial ratio γ is related to the true axial ratio Γ by the expression:

$$\gamma = [(P+Q-R)/(P+Q+R)]^{\frac{1}{2}},$$

where
$P = \sin^2\theta\,(1+\Gamma^2\cot^2\theta)$,
$Q = \sec^2 i\,\cos^2\theta\,(1+\Gamma^2\tan^2\theta)$,
$R = (P-Q)^2+4H^2$,
$H = \sec i\,(1-\Gamma^2)\sin\theta\cos\theta$,
θ = angle between the major axis of the ellipse and the horizontal plane (or inclination of the minor axis),
i = angle of incidence of Jupiter radiation.

Figure 3 shows this relation for an angle of incidence of 37° which was typical for the observations reported here. Faraday rotation along the path will cause the inclination of the ellipse (θ) at the antenna to differ from that at the point of emission on Jupiter by some hundreds of radians. A small change in the total electron content along the path will produce a large change in θ so that in general θ will be changing continuously. If θ changes slowly in time so that it is essentially constant during a burst, then a large number of bursts of a given axial ratio will be observed as a distribution of projected axial ratios which can be calculated from the appropriate curve in Figure 3 by assuming that all values of θ are equally probable. Slight complications arise if θ varies during a burst, but this is automatically overcome, as we will see later.

Faraday rotation is also frequency dependent. If the differential rotation over the bandwidth of the receiver is greater than 180° all values of γ for a given Γ will be averaged. The mean projected axial ratios ($\bar{\gamma}$) as a function of incidence angle (i) for several values of true axial ratio (Γ) are shown in Figure 4.

An expression for the Faraday rotation fading rate is given by Aitchison and Weekes (1959). If longitudinal propagation is assumed and a typical effective value of total electron content (I) of about 30×10^{12} cm^{-2} is substituted, this becomes

$$2\frac{\partial\theta}{\partial t} = 4\times 10^4(If^2)^{-1}\frac{\partial}{\partial t}(I \sec i),$$

where θ is measured in revolutions and the frequency (f) in megacycles per second. Substituting f = 10 Mc/s, the average fading rate caused by the variation of incidence angle (i) over the 5-hr observing periods centred on transit would produce a fading rate of about one per minute. A 30% change in I (at constant i) spread over the same period would produce a similar rate. This fading period is much longer than typical

Jupiter bursts. An expression for the rate of change of rotation with frequency can be similarly derived:

$$\partial\theta/\partial t = -8 \times 10^4 f^{-3} \sec i \qquad \text{rev}/(\text{Mc/s}).$$

For $f = 10$ Mc/s and $\sec i = 1 \cdot 25$ we find that θ will change by 180° over a bandwidth of 5 kc/s.

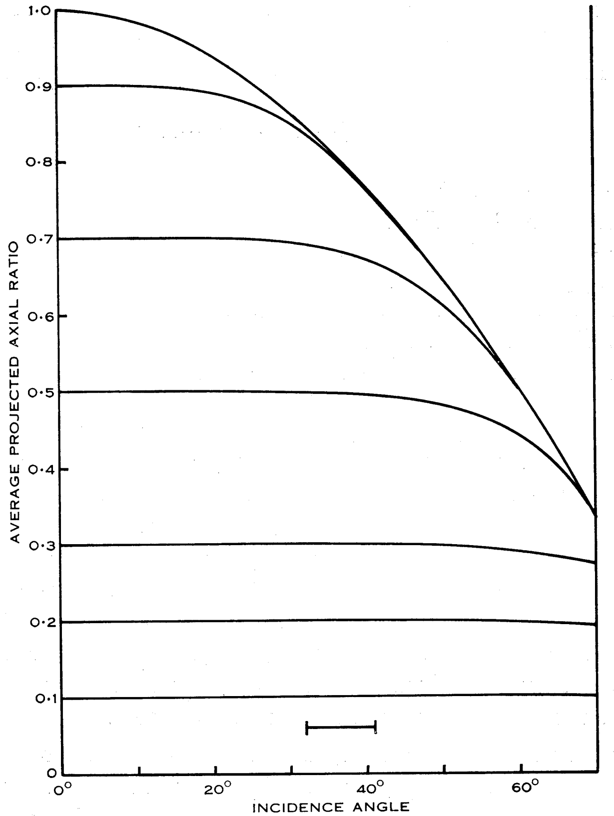

Fig. 4.—Projected axial ratio averaged over all ellipse inclinations as a function of the angle of incidence for various actual axial ratios.

Since the receiver bandwidth was about 4 kc/s, the projected axial ratios will be averaged by the receiver, giving the corrections indicated in Figure 4. Over the range of incidence angles which apply to these observations (as indicated by the limit bar in Fig. 4), and for $\Gamma < 0 \cdot 7$ we find $\bar{\gamma} \approx \Gamma$ to within the limit of the scaling errors. This also applies if the amount of Faraday rotation has been underestimated. If it has been overestimated values of γ will not be completely averaged by the receiver. This will produce a broadening effect, since each value of Γ produces a range of γ. However, for the distribution as shown in Figure 11 the total corrections would be less than the statistical errors.

Apart from projection effects, the observed axial ratio will be smaller than those emitted on Jupiter if some bursts of opposite polarization are superimposed on the record. In this way apparent ratios near zero could be produced by coincident and oppositely polarized bursts of relatively high axial ratio.

A similar and potentially more serious effect may be irrelevant. Roberts (1963) has pointed out that polarizations deduced from measurement of only the two circular components could be interpreted in two ways: pure elliptical polarization or a mixture

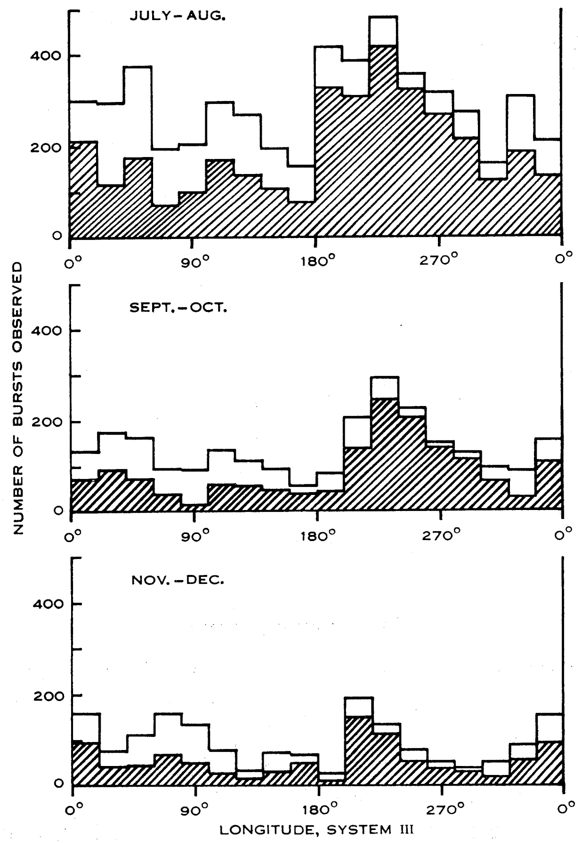

Fig. 5.—Histograms of Jupiter bursts for three observing periods. The shaded portions correspond to bursts polarized in the right-handed sense.

of pure circular plus random polarization. He pointed out that this could be resolved by measuring the random component as well. However, this is difficult at decametre wavelengths because the Faraday rotation is large and is both frequency and time dependent. Thus, at 10 Mc/s, for the Faraday rotation estimated above, the orientations of ellipses would be completely randomized over a bandwidth of about 5 kc/s or a time constant of about 1 min. Thus physically realizable polarimeters would tend to see only circular plus random polarization when pure elliptical polarization was incident. In view of this, one or other interpretation must be chosen on other grounds. The former (pure elliptical) is chosen here.

An alternate method of studying polarization variations is to count the relative proportions of L.H. and R.H. bursts. This method does not suffer from any of the effects mentioned above, since none of them can reverse the sense of polarization. It has the additional advantage of involving only simple counting instead of two measurements and a calculation for each burst. Much of the following discussion is based on this method. The effect of imbalance between the L.H. and R.H. channels, which can occur both in the equipment and in the Earth's ionosphere, leading to a zero shift in axial ratio, will be discussed later.

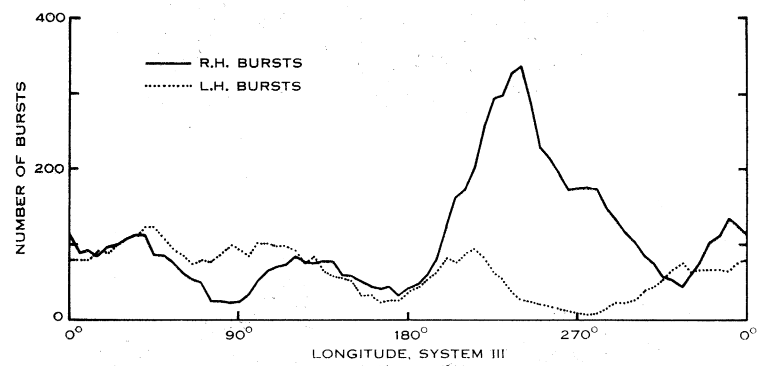

Fig. 6.—Smoothed occurrence rate of right-handed and left-handed bursts in September–October.

IV. Observations

Polarimeter records of Jupiter bursts were obtained from July to December 1962. This period was divided into three periods of from July 4 to August 28, August 28 to October 8, and November 21 to December 22. Histograms of burst occurrence in 20° intervals of longitude are shown for the three periods in Figure 5. The number of R.H. bursts is indicated by the shaded areas while that for L.H. bursts is superimposed as white areas. The histograms for the three periods are similar, bearing in mind the statistical error and the different lengths of the observing periods. Thus the bursts occurring in the September–October period, which were scaled in greater detail, should be reasonably typical. For this period the L.H. and R.H. power components of circular polarization were measured, and the (apparent) axial ratio calculated, for each burst. Intervals of five degrees of longitude were used, but to reduce statistical fluctuations centred running means over 25° were calculated.

Figure 6 shows the occurrence rate of L.H. and R.H. bursts for the September–October period. The occurrence rate of R.H. bursts shows a pronounced variation with longitude with peak occurrence at 240°. Nearly half (48%) of all R.H. bursts occurred within 40° of this peak. The occurrence rate of L.H. bursts shows less variation and a number of subsidiary peaks, the largest occurring at about 40°.

The sum of the peak powers of all bursts occurring within 25° ranges of longitude are plotted (dots) at 5° intervals in Figure 7. The L.H. and R.H. components have been added. The burst occurrence rate is plotted in a similar way (crosses) on the same graph. In general the two curves follow the same trends though the "total power" seems to be more sensitive to longitude than burst occurrence rate and has a greater maximum to minimum ratio.

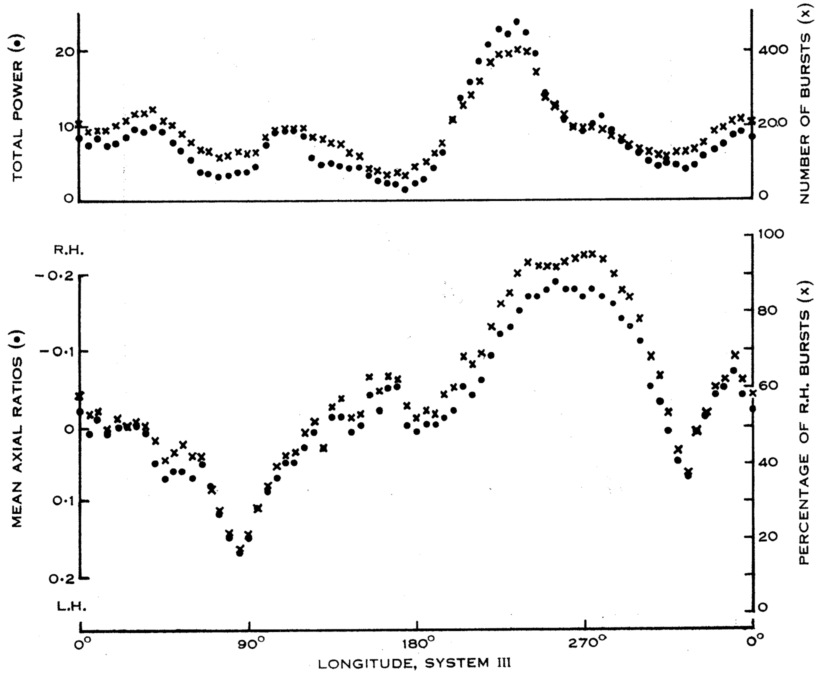

Fig. 7.—Smoothed longitude variation of total power and mean axial ratio (dots), and of the burst occurrence rate and the proportion of bursts which were polarized in the right-handed sense (crosses).

Also shown in Figure 7 are the mean algebraic (positive and negative) axial ratios (dots) of bursts occurring within 25° ranges of longitude and the percentage of these bursts which were polarized in the R.H. sense (crosses). Both show a pronounced and very similar variation with longitude. We would expect some relation between the two for the following reason. The mean algebraic axial ratio is defined as

$$\bar{\Gamma}=\frac{\Sigma\,\Gamma}{N},$$

where N is the number of bursts observed. If the bursts are separated into L.H. and R.H., we have:

$$\bar{\Gamma}=\frac{\Sigma\,\Gamma_{\mathrm{L}}+\Sigma\,\Gamma_{\mathrm{R}}}{N_{\mathrm{L}}+N_{\mathrm{R}}}$$

$$=\frac{N_{\mathrm{L}}\bar{\Gamma}_{\mathrm{L}}+N_{\mathrm{R}}\bar{\Gamma}_{\mathrm{R}}}{N_{\mathrm{L}}+N_{\mathrm{R}}}.$$

Variation of $\bar{\Gamma}$ can be produced by variation of either (or both) N_L/N_R or $\bar{\Gamma}_L/\bar{\Gamma}_R$. It is quite clear from Figures 6 and 7 that N_L/N_R is not constant, so we will consider $\bar{\Gamma}_L = -\bar{\Gamma}_R = \bar{\Gamma}_A$. Then

$$\bar{\Gamma} = \frac{N_L - N_R}{N_L + N_R} \cdot \bar{\Gamma}_A = \left(1 - 2\frac{N_R}{N}\right) \cdot \bar{\Gamma}_A.$$

Thus, if the distribution of absolute values (signs disregarded) of axial ratio is not

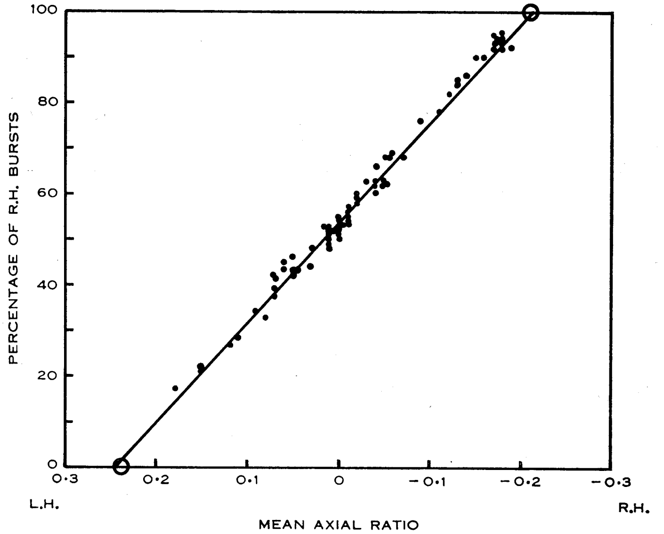

Fig. 8.—Correlation of the mean axial ratios and the percentage of right-handed bursts. The circles at 0% and 100% are the mean axial ratios of left-handed and right-handed bursts respectively.

Table 1

MEAN AXIAL RATIOS OF L.H. AND R.H. BURSTS

Longitude	Left Hand			Right Hand		
	$\Sigma\Gamma$	N	$\bar{\Gamma}$	$-\Sigma\Gamma$	N	$-\bar{\Gamma}$
0°– 60°	63·25	237	0·27	51·20	230	0·20
60°–120°	51·00	210	0·24	20·45	110	0·185
120°–180°	27·95	120	0·23	29·25	141	0·21
180°–240°	31·15	157	0·20	81·15	423	0·19
240°–300°	8·70	41	0·21	104·15	459	0·225
300°–360°	34·55	148	0·235	40·90	193	0·21
0°–360°	216·60	913	0·237	327·10	1556	0·210

dependent on longitude, the algebraic mean axial ratio will be a linear function of the percentage of R.H. bursts (N_R/N).

The correlation of these two quantities is shown in Figure 8. A linear relationship is a good fit. Mean axial ratios of L.H. and R.H. bursts considered separately and for six longitude intervals of 60° are shown in Table 1.

It is seen that there is little or no systematic variation of average axial ratio with longitude for bursts of either sense of polarization. The cyclotron theory (Ellis and McCulloch 1963) predicts a slight tendency for $\bar{\Gamma}$ to follow N according as

$$\Sigma \, \Gamma \propto N^{1 \cdot 05}.$$

The relation is tested in Figure 9 by plotting the information given in Table 1. The

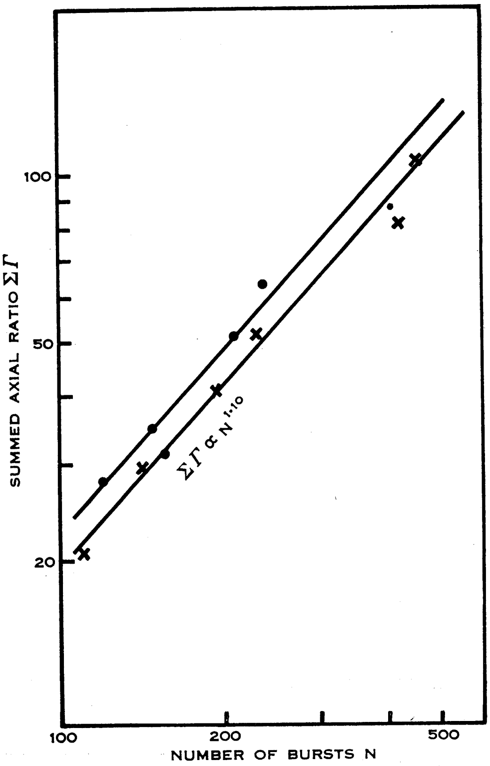

Fig. 9.—Correlation of summed axial ratio and occurrence rate of bursts. Left and right-handed bursts are plotted as dots and crosses respectively. For the small dot both scales should be reduced by a factor of ten.

exponent for best fit appears to be $1 \cdot 10$, which is probably not significantly different from that predicted. A similar prediction of the cyclotron theory is that the total power (Σ P) be related to the number of bursts by the relation

$$\Sigma \, P \propto N^{1 \cdot 3}.$$

The exponent for best fit of the data in Figure 7 is seen in Figure 10 to be $1 \cdot 51$. The difference, if significant, could be due to the increased probability of coincidence of bursts when the occurrence rate is large.

It will be noted from Figure 1 that not all the amplification of the signals from Jupiter was common to both polarization components. Gain balance was measured by automatic hourly noise generator calibrations, though no special precautions were taken to maintain exact balance. Since the relation between measured axial ratio

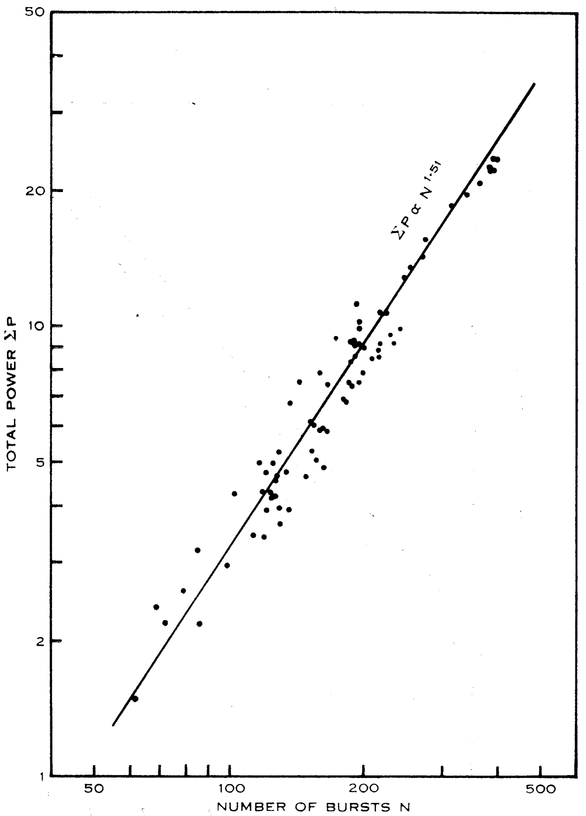

Fig. 10.—Correlation of the total power and the occurrence rate of bursts.

and power ratio (r) is quite closely logarithmic for values of r between $0 \cdot 1$ and 10, a small amount of imbalance would affect nearly all values of measured axial ratio by an algebraically additive constant. That is, it would shift the zero of the axial ratio scale. The zero chosen was deduced from the noise calibrations. For this zero the Galactic noise has an apparent axial ratio of about $0 \cdot 043$. This suggests a small amount of differential absorption in the Earth's ionosphere, assuming that Galactic noise is completely randomly polarized. The absorption is not necessarily the same for Jupiter radiation, since the brightest parts of the Galaxy were lower in the sky than Jupiter during these observations.

It is interesting to note that if a correction of 0·025 is used we find that, averaged over all longitudes, $\bar{\Gamma}_L = -\bar{\Gamma}_R = 0{\cdot}212$. Also the regression line in Figure 8 now passes through the point $\bar{\Gamma} = 0$, $N_R/N = 50\%$, and the two regression lines in Figure 9 (for L.H. and R.H. bursts respectively) coincide. This zero correction has been applied in the histogram of absolute values of axial ratio shown in Figure 11. The absolute axial ratio distribution does not appear to be a function of longitude, so this histogram was compiled from values from all longitudes. The projection correction has not been applied, as it would have very little effect. The observed distribution is similar in shape to that predicted by Ellis and McCulloch, if it is assumed that apparent axial ratios below about 0·2 are produced by superimposition of bursts of higher axial ratio but of opposite sense of polarization. The position of the predicted distribution on the axial ratio scale depends on the model used rather than on the theory.

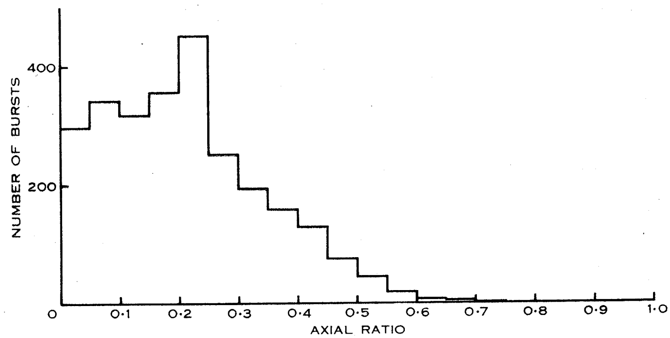

Fig. 11.—Histogram of absolute values (both left and right taken positively) of axial ratio. The zero correction has been applied but the shape of the distribution makes the projection correction unnecessary.

V. Discussion

On the cyclotron theory (Ellis and McCulloch 1963) the configuration of the Jupiter magnetic field in longitude can be deduced from observations of the longitudinal variation of burst occurrence, preferably at a number of frequencies. Much additional information is provided by polarization measurements. Thus, by considering the L.H. and R.H. burst occurrence rates separately, as in Figure 6, both the regular or dipole component and the anomalous components can be resolved into hemispheres. It is felt that the polarization data obtained so far are not sufficient for a detailed analysis of field configuration. Intercomparison of the three histograms in Figure 5 shows that much of the fine structure of the occurrence rates is statistical error. However, some conclusions can be drawn from the broad features which persist through these three histograms.

The main features of the occurrence rates in Figure 6 are a large and fairly narrow peak for R.H. bursts at about 240° and a smaller and broader peak for L.H. bursts at about 40°. The L.H. peak is somewhat larger and more prominent in the July–August histogram of Figure 5. If the occurrence rates are not masked by anomalous peaks, this would give the positions of the north-seeking and the south-seeking poles respectively. Decimetre observations by Morris and Berge (1962) show that the longitudes of the poles are $230 \pm 10°$ for the pole in the northern hemisphere and $50 \pm 10°$ for that in the southern hemisphere, after conversion to the longitude system used here. Observations by Roberts and Komesaroff (Bolton 1963) show these poles at 215° and 35° respectively. Both of these are in reasonable agreement with the positions deduced from Figure 6, and further indicate that the sense of the magnetic field of Jupiter is opposite that of the Earth, for the north-seeking magnetic pole is located in the northern hemisphere.

The fact that the R.H. or northern hemisphere peak is two to three times the L.H. or southern hemisphere peak may be significant. The large R.H. peak could be a combination of a "polar" peak at about 220° and an anomalous peak at about 260°. The data considered by Ellis and McCulloch support this interpretation. On the other hand an asymmetry in the polar peaks (without localized anomalies) of about this amount would be produced if the magnetic dipole is displaced along its axis towards the northern hemisphere by an amount (0·05 times the planet's radius) similar to that of the Earth. This asymmetry would increase with frequency and produce different cut-off frequencies for the two polarizations. The observed cut-off frequencies are around 38 Mc/s (Barrow 1963) for R.H. radiation and around 22 Mc/s (Carr *et al.* 1961) for L.H. radiation.

Such displacements of the dipole are not inconsistent with the decimetre observations. In particular, it should be noted that the decimetre observations only locate the longitudes of the poles if the magnetic and rotation axes are coplanar. Thus, if the dipole is displaced about 0·05 radii in a direction perpendicular to both axes, the longitudes of the poles (using the Morris and Berge data) would be 214° and 34° (or 246° and 66°) and thus only 148° apart. More data are required for accurate location of the dipole position. Polarization measurements at a low frequency (such as 5 Mc/s), where contributions from dip anomalies are very small (Ellis and McCulloch 1963), may resolve this.

VI. Acknowledgments

The author is indebted to Professor G. R. A. Ellis for many helpful discussions and suggestions, to Mr. M. L. Urquhart for deriving the axial ratio projection expression, and to Mr. G. T. Goldstone for building and operating the polarimeter.

VII. References

Aitchison, G. J., and Weekes, K. (1959).—*J. Atmos. Terr. Phys.* **14**: 236–48.
Barrow, C. H. (1963).—*Nature* **197**: 580.
Bolton, J. G. (1963).— *Proc. Inst. Radio. Engrs. Aust.* **24**: 106–12.
Carr, T. D., Smith, A. G., Pepple, R., and Barrow, C. H. (1958).—*Astrophys. J.* **127**: 274.
Carr, T. D., Smith, A. G., Bollhagen, H., Six, N. F., Jr., and Chatterton, N. E. (1961).—*Astrophys. J.* **134**: 105–25.
Dowden, R. L. (1963).—*Proc. Inst. Radio. Engrs., N.Y.* **51**: 231.
Ellis, G. R. A. (1962).—*Aust. J. Phys.* **15**: 344–53.
Ellis, G. R. A., and McCulloch, P. M. (1963). *Aust. J. Phys.* 16: 380–97.
Morris, D., and Berge, G. L. (1962). *Astrophys. J.* **136**: 276.
Roberts, J. A. (1963).—*Planet. Space. Sci.* **11**: 221–59.